NANO LETTERS

2006
Vol. 6, No. 7
1496−1501

Structural Basis for Near Unity Quantum Yield Core/Shell Nanostructures

James McBride,[†] Joe Treadway,[§] L. C. Feldman,[‡,||] Stephen J. Pennycook,[||] and Sandra J. Rosenthal*[,†,||]

Department of Chemistry and Department of Physics and Astronomy, Vanderbilt University, Nashville Tennessee, Quantum Dot Corporation, Hayward, California, and Oak Ridge National Laboratory Condensed Matter Sciences Division, Oak Ridge, Tennessee

Received May 2, 2006; Revised Manuscript Received May 31, 2006

ABSTRACT

Aberration-corrected Z-contrast scanning transmission electron microscopy of core/shell nanocrystals shows clear correlations between structure and quantum efficiency. Uniform shell coverage is obtained only for a graded CdS/ZnS shell material and is found to be critical to achieving near 100% quantum yield. The sublattice sensitivity of the images confirms that preferential growth takes place on the anion-terminated surfaces. This explains the three-dimensional "nanobullet" shape observed in the case of core/shell nanorods.

Nanomaterials are destined to be the building blocks for future innovative devices because of their promise of revolutionary advances in photovoltaics, fuel cells, material composites, catalysis, and even drug discovery.[1−3] Fluorescence imaging is one such field that has been advanced with the recent introduction of highly fluorescent quantum dots.[4−7] The signature properties of quantum dots, including their unique size-dependent tunable emission, resistance to photobleaching, and high brightness, enable extended data collection periods and facile multiplexing experiments.[8−10] A significant hurdle in the future development of precisely engineered nanostructures with optimized properties is the lack of a means for determining structure and composition at the atomic level. For example, even a single monolayer of surface passivating inorganic shell on a nanocrystal core can increase the fluorescence quantum yield by a factor of 3.[11] Although the addition of a few monolayers can be confirmed using traditional characterizing techniques such as X-ray diffraction, transmission electron microscopy, and X-ray photoelectron spectroscopy, several important questions still remain, such as the actual total coverage of the shell, whether all the nanocrystal surfaces are equally coated, and if there are any defects at the shell interface or on the surface. To design robust core/shell quantum dots, a technique is needed to characterize the shell and shell surface with greater sensitivity. Atomic number contrast scanning transmission electron microscopy (Z-STEM) provides an unmatched ability to achieve structural and chemical information from individual nanostructures at the atomic level.[12] For example, Z-STEM tomography was used recently to determine the three-dimensional structure of less than 10 nm tin quantum dots embedded in silicon with cubic nanometer resolution.[13] We have applied Z-STEM to characterize the shell quality of a series of CdSe based core/shell materials with varying quantum yields in order to reveal the physical nature of the inorganic shell at the atomic level. The intensity difference between the core and shell seen in Z-STEM images allows precise characterization of shell shape, coverage, chemical composition, and the presence of any extended defects. The images clearly reveal the structural requirements for 100% quantum efficiency. Furthermore, the sublattice resolution of the images reveals the nanocrystal polarity directly, showing the anion-terminated faces to be preferential for growth. This growth mechanism explains the observed nanorod morphology.

Z-STEM uses a high angle annular dark field (HAADF) detector to collect an incoherent image, a direct image of the object's structure.[12,18−21] Unlike traditional HRTEM that uses phase-contrast imaging to gain insight into the crystalline nature of the particles, the intensity seen in the Z-STEM images depends on the scattering power of the atom being imaged, yielding chemical information simultaneously with structural position. The combination of these two properties makes Z-STEM an ideal tool for studying core/shell structures at the atomic level. The mass difference between the core and shell material manifests itself as a clear change in intensity in the raw images. Coreless, or "dark" particles, which are nanocrystals that absorb light yet do not contribute

* Corresponding author. E-mail: sandra.j.rosenthal@vanderbilt.edu. Address: Chemistry Department, Vanderbilt University, VU Station B, Box 351822, Nashville, TN 37235-1822. Phone: 615-322-2633. Fax: 615-343-1234.

[†] Department of Chemistry, Vanderbilt University.

[‡] Department of Physics and Astronomy, Vanderbilt University.

[§] Quantum Dot Corporation.

[||] Oak Ridge National Laboratory Condensed Matter Sciences Division.

10.1021/nl060993k CCC: $33.50
Published on Web 06/09/2006

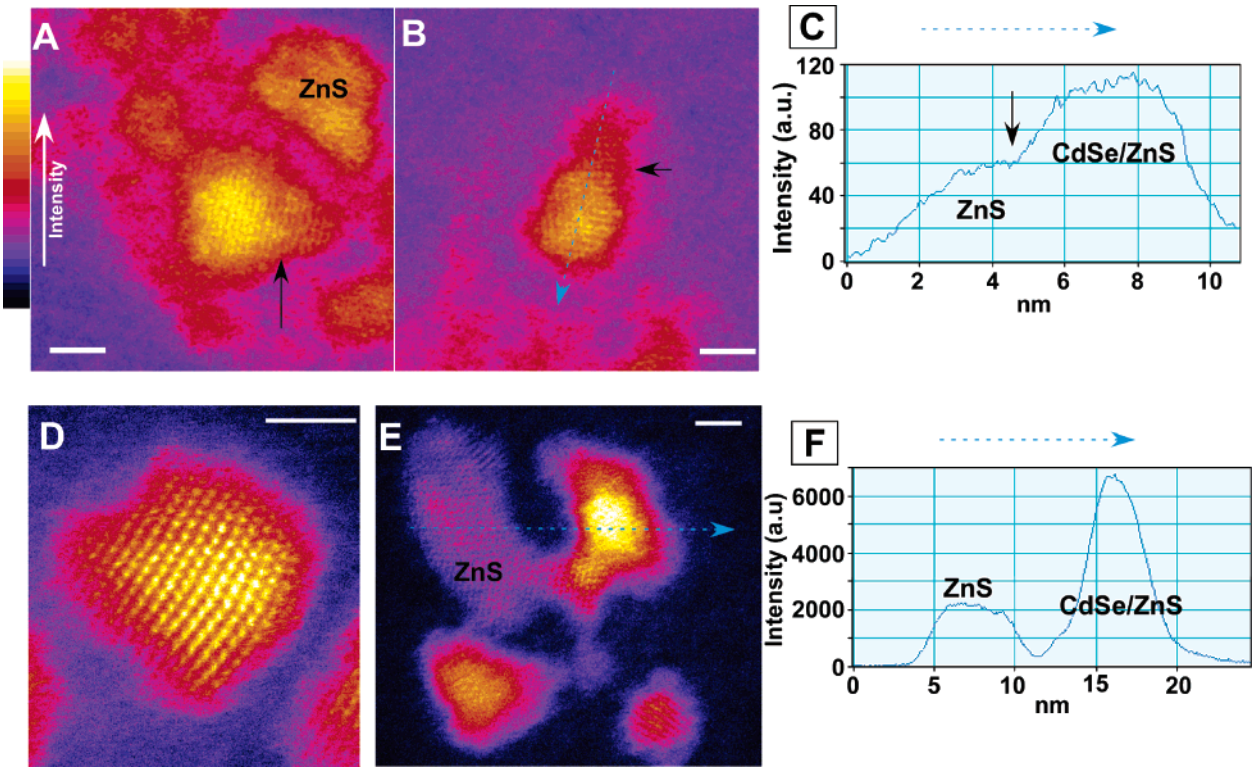

Figure 1. Z-STEM of CdSe/ZnS core/shell nanocrystals. The images (A and B) are of a core/shell sample with a quantum yield of 34%. Contrast can be seen between the heavier core material and the lighter shell material. The line profile (C) shows the interface between core and shell clearly. The lattice resolved image (D) of a graded CdSe/CdS/ZnS nanocrystal is the first image of a core/shell acquired using an aberration-corrected STEM. This sample had Cd introduced into the shell and showed a quantum yield of 84%. The intensity profile (E) illustrates the ease of identifying dark particles. The line scan (F) shows the intensity difference between a ZnS particle and an equally sized CdSe/ZnS core/shell. The scale bars correspond to a length of 3 nm.

to the desired emission, are identified easily in the same manner. We chose to study CdSe-based cores/shell systems because they have been prepared and characterized in many different ways previously. The purpose of the shell material is to passivate surface trap sites and to energetically confine the electron and hole. Ideally, for every photon that creates an electron and hole pair, one photon is emitted. To ensure radiative electron and hole recombination, a material with a wider band gap than the core is used to coat the surface.[11,17,22−25] In the case of CdSe, ZnS is typically used as the shell material because of its wide band gap. This is an ideal first system for Z-STEM because of the large mass difference between the ZnS shell and the CdSe core.

Core/shell nanocrystals of this type were prepared using standard literature techniques that utilize trioctylphosphine oxide (TOPO) as the surfactant and dimethylcadmium and Se powder mixed with tributylphosphine as the metal precursors.[11] Once the cores were made, the solution was heated again, and a mixture of bis(trimethylsilyl) sulfide and diethylzinc were added to initiate shell growth. The growth was stopped once the fluorescence intensity reached a maximum.

Samples for Z-STEM were prepared by dropping a dilute solution of core/shell nanocrystals onto an ultrathin carbon-coated TEM grid (Ted Pella, Inc.) and allowing it to evaporate. Z-STEM images were taken on a VG Microscopes' HB603U STEM operating at 300 kV, fitted with a Nion aberration corrector (www.nion.com). This instrument has demonstrated direct resolution at 0.78 Å with information transfer to 0.6 Å.[12]

Figure 1a shows a CdSe/ZnS core/shell nanocrystal, prepared using standard literature preparation with a measured quantum yield of 34%.[25]

The nanocrystal in the center of the raw Z-STEM image features a bright core with a fainter shell encircling it. Lattice fringes seen on the shell indicate that it is crystalline; however, the shell is aspherical and coats the core unevenly. From this image, the existence of coreless particles, presumably ZnS particles that nucleated during shell growth, can be confirmed. These dark particles can be identified clearly by the uniform intensity across the particle. Also, a large amount of excess starting material is associated with the core/shell nanocrystals, which is surprising to find after several washings. Figure 1b shows an extreme case in which the shell grew in only one direction. The Se-rich, (001′) face of CdSe is typically the most reactive and therefore the most likely place for initial shell growth to occur.[19,24,26,29] This leads to a competitive growth process that often leaves the remainder of the core with little or no shell coverage such as the core/shell shown in Figure 1b. Figure 1c shows a line profile along the *C* axis of the core/shell in Figure 1b, illustrating the intensity change going from shell to core. The shell clearly predominantly covers one surface of the core. The interface between core and shell has been marked with a black arrow. An extreme excess of ZnS precursors was used in order to try and passivate all facets of the core,

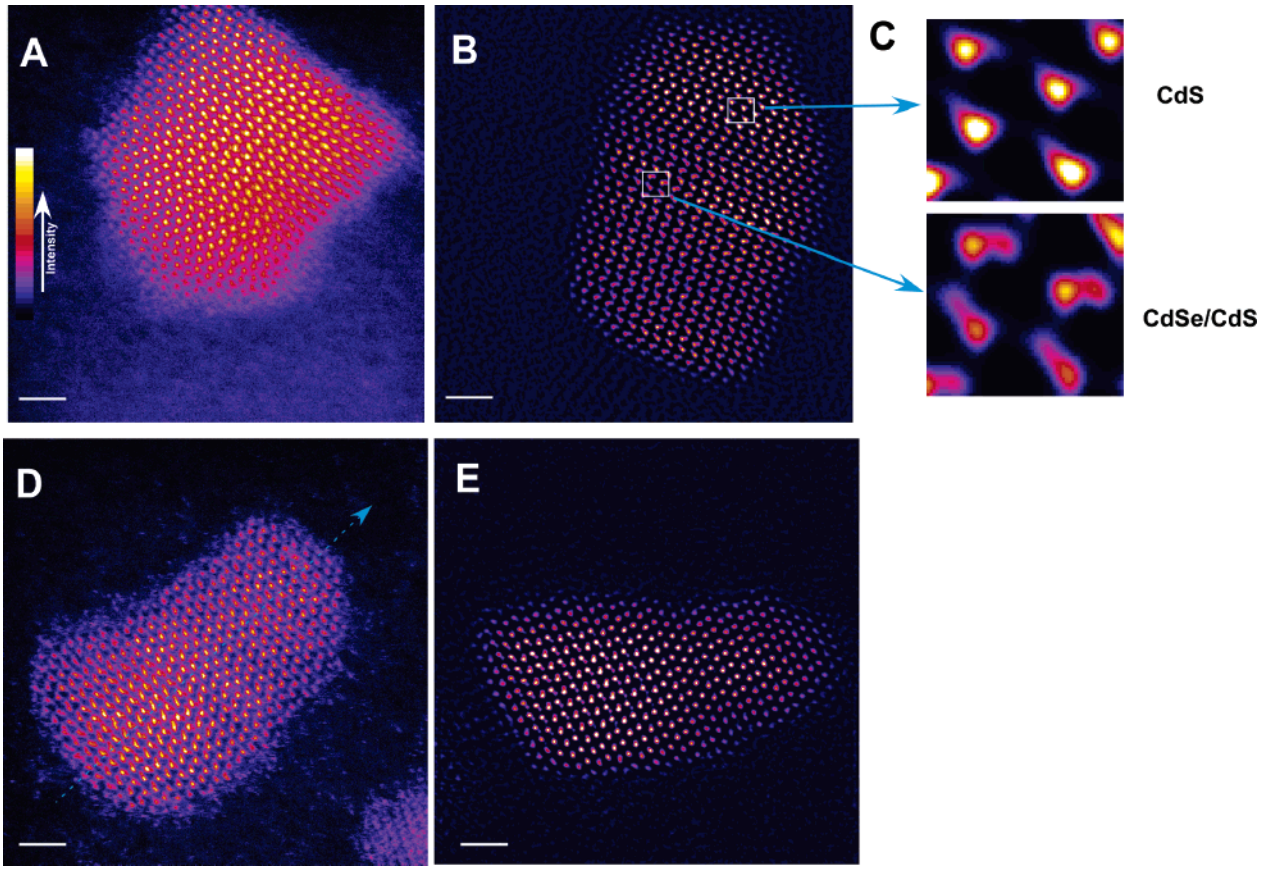

Figure 2. Z-STEM images of CdSe/CdS/ZnS core/shell rods. The images (A and B) are Z-STEM images of the 655 nm emitting commercial core/shell rods from Quantum Dot Corporation. The mass contrast between core and shell has been reduced, indicating that the shell material is predominantly CdS. The atomic dumbbells in the image can be used to assign the flat end of the nanorod as the (001) surface. The difference between the dumbbell intensities (C) between the core/shell and the shell material indicates a change of material composition. The images (D and E) are Z-STEM images of 605 nm emitting commercial core/shell rods from Quantum Dot Corporation. They exhibit the bullet shape to a lesser extent. Both of these samples have quantum yields approaching 100%. The images (B and E) have been Fourier filtered to reduce background noise. The scale bars correspond to a length of 2 nm.

causing the nucleation of ZnS particles that were found in this sample.

The thickness of a defect-free shell is limited by the 11% lattice mismatch between CdSe and ZnS.[11,25] To grow thick, defect-free shells, a lower lattice mismatch is desirable. Because the CdSe to CdS lattice mismatch is only ~3.6%, Cd was added to the shell growth process to improve the quality of the shell coverage.[21] Rutherford backscattering spectroscopy (RBS) analysis was used to confirm the addition of Cd to the sample, indicating that the atomic ratio of Zn to Cd was reduced to 3:1 from the 8:1 value found in the literature-prepared sample.[28] The resulting structure is a gradient core/shell with a CdSe core and a mixture of CdS and ZnS as the shell. The gradient core/shell sample had a quantum efficiency of 84%, an improvement greater than a factor of 2 over the literature-prepared sample. Figure 1d is a lattice-resolved Z-STEM image of a gradient core/shell nanocrystal. The addition of Cd to the shell has resulted in a reduction in the intensity contrast between core and shell, while the overall core/shell exhibits a blocky shape compared to the ovoid shape of the core starting material. Other images still show the occasional ZnS particle, as demonstrated in Figure 1e. This image features a core/shell nanocrystal associated with a long ZnS nanocrystal. The line profile, Figure 1f, illustrates just how easily ZnS particles can be identified by the image intensity. Because there is no change in the chemical composition, the ZnS particle has a nearly flat intensity profile while the neighboring core/shell particles have Gaussian-like intensity profiles.

The gradient shell method was used to coat CdSe nanorods with aspect ratios near 2:1. It is now well understood that the formation of nanorods is the result of ligand-directed preferential growth along a single axis.[26] This presents a challenge for traditional shell synthetic approaches because this axis remains preferred during shell deposition. Although some limited success has been reported in the past, high-quality rodlike core/shells exhibiting high emission efficiencies have proven to be essentially impossible by traditional methods.[27] However, core/shell nanorods can reproducibly be prepared with efficiencies of 100% using the gradient shell method. Because the Cd content in the shell has again been increased in these cases (as determined by RBS), the Z-STEM images of these core/shells in Figure 2 show reduced contrast between core and shell.

However, clear contrast can be seen between the intensity of the selenium and sulfur from the atomic "dumbbells" in

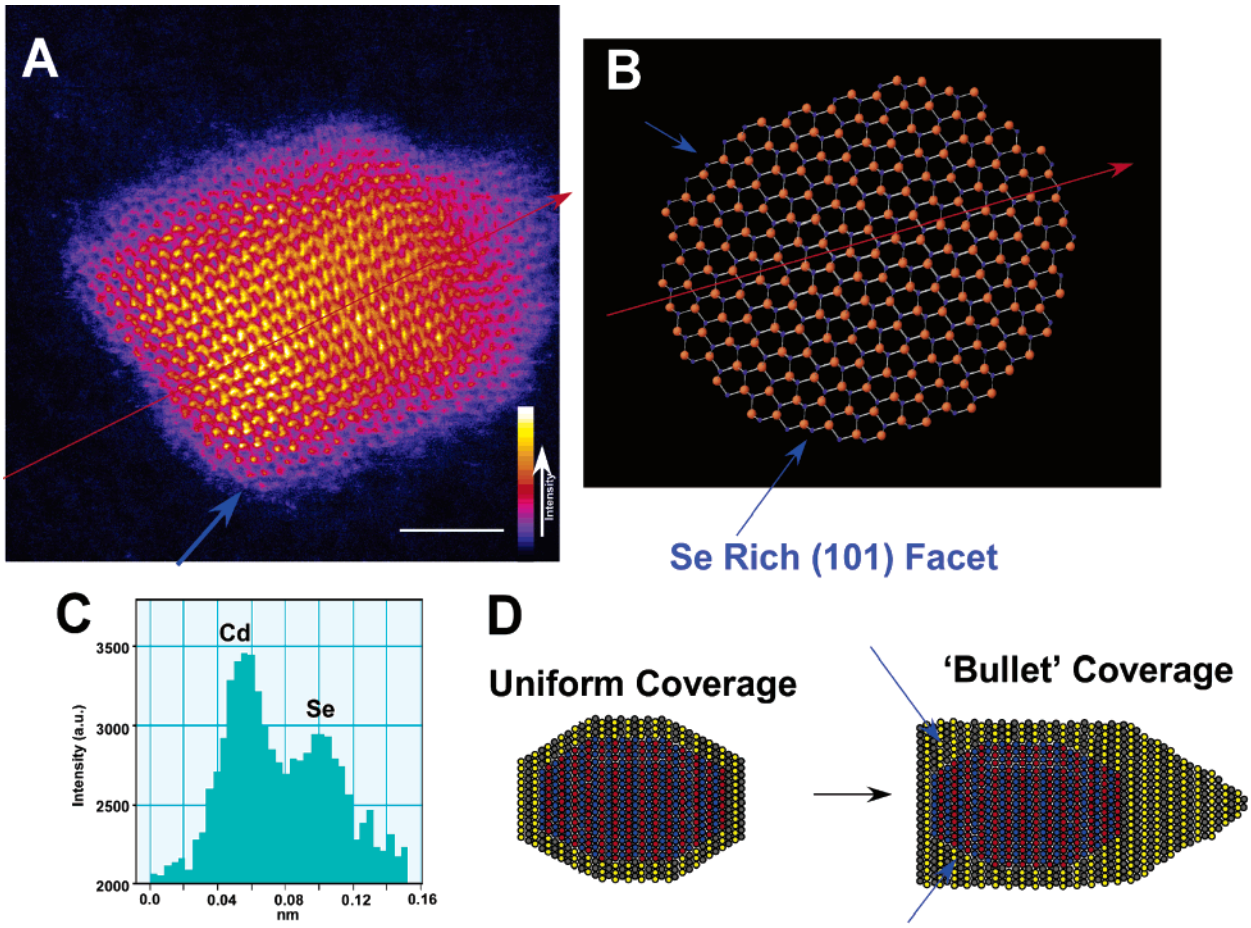

Figure 3. Preferential facet coverage. The high magnification view of a nanobullet (A) definitively reveals the sublattice polarity in the CdS and CdSe regions from the relative intensity, shown by line traces (C). A model structure commonly assumed for nanocrystals (B) can be directly compared to the image. Comparing the image with the model illustrates how the shell must be growing at a higher rate only on the Se rich facets to form the bullet shape, as shown schematically in D. The red arrows indicate the *c* axis, and blue arrows indicate the Se-rich (101) facets. The scale bar in A corresponds to a length of 3 nm.

the images. This is illustrated by the noticeable change in the appearance of the alternating hexagonal dumbbells going from the center of the particle to the tip. Interestingly, the overall morphology deviates strongly from a homogeneous shell coating. The core/shell shape is that of a "bullet", capped with a flat surface on one end while forming a point on the other, as demonstrated by the images in Figure 2a and b. Figure 2c illustrates the intensity difference from the atomic dumbbells at the center of the core/shell rod from those of the tip. The reduction of the anion intensity suggests that the tip is primarily CdS because of the lower scattering power of sulfur atomic columns.

It is important to note that the 605-nm emitting core/shell rods, Figure 2d and e, also have a quantum yield of nearly 100% but have much less shape homogeneity, appearing narrower and more elongated. The shell covering the (001′) facet is nearly as large as the core particle. The filling of the (101) facets is not as evident in the majority of these core/shell rods; however, the shell material still covers the Se-rich faces preferentially.

For the first time, this extreme level of atomic detail can be applied to identify specific facets in the image. This is important because the CdSe nanocrystal facets are not chemically equivalent, which can explain why the coating of the shell is not uniform, as illustrated in Figure 3.

Once the alternating intensity pattern of the Cd and Se dumbbells is identified (Figure 3a), we can then assign one end of the rod as the Se-rich (001′) face and the other as the Cd-rich (001) face. Then the image can be compared to a model of the CdSe core, such as that found in Figure 3b, to identify the remaining surfaces. The image in Figure 3a exhibits the typical nanobullet shape with a nearly perfectly flat end opposite a pointed end. Using the atomic dumbbells, we can definitively assign the pointed end of the nanorod as the anion-rich (001′) face. This supports predictions in the literature that the selenium-rich face is the primary growth face for the CdSe core.[19,24,26,29] The facets with the next highest concentration of Se surface sites are the (101′) facets located near the flat end of the nanobullet. Interestingly, to achieve the unique bullet shape, these corner (101′) facets must also grow at a faster rate than the side (100) surfaces. The shell appears to be thinnest on the Cd-rich (001) and (100) surfaces, with an average coverage of a monolayer or two, while the (101′) facets have about 4−5 monolayers

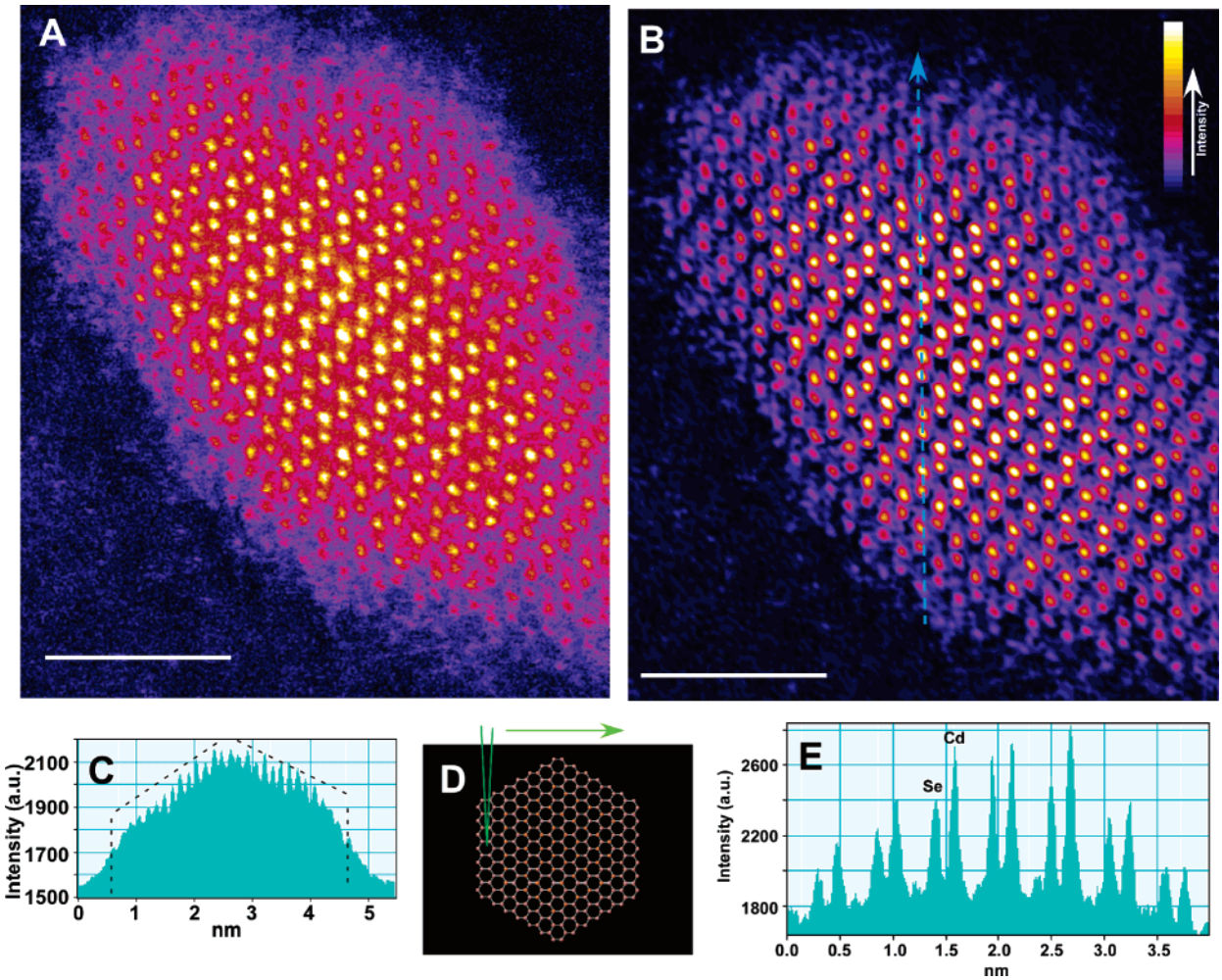

Figure 4. Z-STEM of the (010) face of a 605-nm emitting core/shell rod. The raw image (A) is a Z-STEM image of a core/shell rod with all the atomic dumbbells resolved. To reduce the noise in A, the image was Fourier filtered (B). This orientation is rather unlikely to be found because the nanorod must rest on an edge. The line profile (C) across the raw image illustrates the intensity changes across the core/shell rod that outline the facet that is coming out of the plane of the image, as illustrated by the model (D) with the electron probe represented by the green "v". The line profile (E) shows the resolved atomic dumbbells illustrating the mass contrast seen in the image. The scale bars in A and B correspond to a length of 1.5 nm.

and the (001′) facet has anywhere from 6 to 15 monolayers. The growth mechanism clearly selects the anion surface sites.

The last image, Figure 4a, shows a CdSe/CdS core/shell nanorod orientated with the (010) face parallel to the surface plane. The atomic dumbbells are clearly resolved in the raw image and can be assigned easily by their mass contrast. The polarity of the sublattice is clearly continuous throughout the core and shell, although also notice that there is a small cubic intergrowth toward the point. In Figure 4b, the noise from the image has been reduced by a Fourier filter in order to better show the mass contrast and the facets in the image. This rod is resting on an edge, as illustrated by the nanocrystal model, Figure 4d. However, the image does provide a unique opportunity to illustrate how structure in the *z* direction can be obtained from the raw image. The intensity profile in Figure 4c beautifully outlines the faceted shape of the nanocrystal surface in the *z* direction that coincides with this orientation. Amazingly, in this single image we can see the atomic structure, identify specific facets, and determine the nanorod's three-dimensional shape.

The structural details revealed in the Z-STEM images together with the near unity quantum yield indicate that defect-free shell coverage is as important as band-gap engineering considerations in determining the quality of quantum dots. High quantum efficiency depends not only on the reduction of dark particles but also on a uniform and epitaxial shell coating. Additionally, because the shell grows preferentially on certain surfaces, the efficiency also depends on the quality and stability of the ligand coverage on surfaces that have little shell. A wealth of core morphologies and compositions are now readily available, and the challenge, at least within the field of fluorescence, is to discover methods that combine the useful attributes of multiple shell materials. In the pursuit of the best structures, it is critical to understand not only composition but also the 3D arrangement of atoms in space. Increasingly, the challenge is to discover very subtle differences at material interfaces, in the way materials are blended, and in the elemental asymmetries in the shells that result from the underlying core structure. Z-STEM promises to be a formidable technique in this historically difficult endeavor.

Acknowledgment. This research was sponsored by the Department of Energy, under contract DE-FG02-02ER45957 and the National Institute of Health, under contract R 01 EB003728-02 and P20-GM72048-02 with Vanderbilt University, and by the Division of Materials Sciences and Engineering, Office of Basic Energy Sciences, U.S. Department of Energy, under contract DE-AC05-00OR22725 with Oak Ridge National Laboratory, managed and operated by UT-Battelle, LLC.

Note Added after ASAP Publication. This article was published ASAP on June 9, 2006. One reference was added and a citation in paragraph 7 of the main text was changed. The revised article was reposted on June 21, 2006.

References

(1) Colvin, V. L.; Schlamp, M. C.; Alivisatos, A. P. *Nature* **1994**, *370*, 354−357.
(2) Nozik, A. J. *Physica E* **2002**, *14*, 115−120.
(3) Wang, Q. Y.; Johnson, J. K. *J. Phys. Chem. B* **1999**, *103*, 4809−4813.
(4) Bruchez, M.; Moronne, M.; Gin, P.; Weiss, S.; Alvisatos, A. P. *Sci. Rep.* **1998**, *281*, 2013−2015.
(5) Chen, F.; Gerion, D. *Nano Lett.* **2004**, *4*, 1827−1832.
(6) Rosenthal, S. J.; Tomlinson, I.; Adkins, E. M.; Schroeter, S.; Adams, S.; Swafford, L.; McBride, J.; Wang, Y.; DeFelice, L. J.; Blakely, R. D. *J. Am. Chem. Soc.* **2002**, *124*, 4586−4594.
(7) Wu, X.; Liu, H.; Liu, J.; Haley, K. N.; Treadway, J. A.; Larson, J. P.; Ge, N.; Peale, F.; Bruchez, M. P. *Nat. Biotechnol.* **2003**, *21*, 41−46.
(8) Alivisatos, A. P. *J. Phys. Chem.* **1996**, *100*, 13226−13239.
(9) Brus, L. E. *J. Chem. Phys.* **1984**, *80*, 4403−4408.
(10) Shiang, J. J.; Kadavanich, A. V.; Grubbs, R. K.; Alivisatos, A. P. *J. Phys. Chem.* **1995**, *99*, 17417−17422.
(11) Peng, X. G.; Schlamp, M. C.; Kadavanich, A. V.; Alivisatos, A. P. *J. Am. Chem. Soc.* **1997**, *119*, 7019−7029.
(12) Nellist, P. D.; Chisholm, M. F.; Dellby, N.; Krivanek, O. L.; Murfitt, M. F.; Szilagyi, Z. S.; Lupini, A. R.; Borisevich, A.; Sides, W. H., Jr.; Pennycook, S. J. *Science* **2004**, *305*, 1741.
(13) Arslan, I.; Yates, T. J. V.; Browning, N. D.; Midgley, P. A. *Science* **2005**, *309*, 2195.
(14) Donega, C. M.; Hickey, S. G.; Wuister, S. F.; Vanmaekelbergh, D.; Meijerink, A. *J. Phys. Chem. B* **2003**, *107*, 489−496.
(15) Kim, S.; Fisher, B.; Eisler, H.; Bawendi, M. *J. Am. Chem. Soc.* **2003**, *125*, 11466−11467.
(16) Mekis, I.; Talapin, D. V.; Kornowski, A.; Haase, M.; Weller, H. *J. Phys. Chem. B* **2003**, *107*, 7454−7462.
(17) Reiss, P.; Carayon, S.; Bleuse, J.; Pron, A. *Synth. Met.* **2003**, *139*, 649−652.
(18) Nellist, P. D.; Pennycook, S. J. *Ultramicroscopy* **1999**, *78*, 111−124.
(19) McBride, J. R.; Kippeny, T. C.; Pennycook, S. J.; Rosenthal, S. J. *Nano Lett.* **2004**, *4*, 1279−1283.
(20) Pennycook, S. J.; Nellist, P. D. *Z-Contrast Scanning Transmission Electron Microscopy*; Rickerby, D., Valdre, G., Valdre, U., Eds.; Kluwer Academic Publishers: The Netherlands, 1999.
(21) Kadavanich, A. V.; Kippeny, T. C.; Erwin, M. M.; Pennycook, S. J.; Rosenthal, S. J. *J. Phys. Chem. B* **2001**, *105*, 361−369.
(22) Talapin, D. V.; Koeppe, R.; Gotzinger, S.; Kornowksi, A.; Lupton, J. M.; Rogach, A. L.; Benson, O.; Feldmann, J.; Weller, H. *Nano Lett.* **2003**, *3*, 1677−1681.
(23) Talapin, D. V.; Rogach, A. L.; Kornowski, A.; Haase, M.; Weller, H. *Nano Lett.* **2001**, *1*, 207−211.
(24) Manna, L.; Scher, E.; Li, L.; Alivisatos, A. P. *J. Am. Chem. Soc* **2002**, *124*, 7136−7145.
(25) Hines, M. A.; Guyot-Sionnest, P. *J. Phys. Chem.* **1996**, *100*, 468−471.
(26) Rempel, J. Y.; Trout, B. L.; Bawendi, M. G.; Jensen, K. F. *J. Phys. Chem. B* **2005**, *109*, 19320−19328.
(27) Manna, L.; Scher, E.; Li, L.; Alivisatos, A. P. *J. Am. Chem. Soc.* **2002**, *124*, 7136−7145.
(28) Taylor, J.; Kippeny, T.; Rosenthal, S. J. *J. Cluster Sci.* **2001**, *12*, 571.
(29) Peng, Z. A.; Peng, X. *J. Am. Chem. Soc.* **2001**, *123*, 1389−1395.

NL060993K